

## SIMULATION OF MHD MIXED CONVECTION HEAT TRANSFER ENHANCEMENT IN A DOUBLE LID-DRIVEN OBSTRUCTED ENCLOSURE

M.M. Billah<sup>a</sup>, M.M. Rahman<sup>b</sup>, R. Saidur<sup>c</sup> and M. Hasanuzzaman<sup>c</sup>

<sup>a</sup>Department of Arts and Sciences,  
Ahsanullah University of Science and Technology (AUST), Dhaka-1208, Bangladesh

<sup>b</sup>Department of Mathematics  
Bangladesh University of Engineering and Technology (BUET), Dhaka-1000, Bangladesh

<sup>c</sup>Department of Mechanical Engineering  
Faculty of Engineering, University of Malaya, 50603 Kuala Lumpur, Malaysia  
E-mail:mmb.edu@gmail.com

Received 20 December 2010, Accepted 12 January 2011

### ABSTRACT

The present numerical study is conducted to investigate MHD mixed convection flow and heat transfer characteristics in a double-lid driven cavity with a heat-generating solid square block. The cavity horizontal walls are adiabatic while both the vertical lids are maintained at a uniform temperature  $T_c$  and velocity  $V_0$ . The present study simulates a reasonable system such as air-cooled electronic equipment with a heat component or an oven with heater. Emphasis is sited on the influences of the block size and position of the block in the cavity. The transport governing equations are solved employing the finite element formulation based on the Galerkin method of weighted residuals. The validity of the current numerical code used is ascertained by comparing our results with previously published results. The computation is carried out for a wide range of relevant parameters such as block diameter, location of the block and Richardson number. Results are presented for the effect of aforesaid parameters on the contours of streamline and isotherm. Besides, the heat transfer rate in terms of the average Nusselt number and temperature of the fluid and block center are offered for the mentioned parametric values. The obtained results demonstrate that the flow and thermal field are strongly influenced by the abovementioned parameters.

**Keywords:** Double-lid driven enclosure, solid square block, mixed convection and finite element simulation.

### 1. INTRODUCTION

Mixed convection in lid-driven cavities are complex problems due to shear flow caused by the movement of moving wall and buoyancy induced flow. The problem is studied earlier for different thermal and flow boundary conditions such as two-sided lid driven cavities, one sided lid-driven cavities from top, bottom or vertical walls, oscillating walls, fully, partially or non-isothermally heated walls etc. (Al-Amiri et al. 2007; Hsu and How, 1999; Omri and Nasrallah, 1999; Manca et al. 2003; Shokouhmand and Sayehvand, 2004, Hasanuzzaman et al. 2009). Obstacle or a partition is used to enhance heat transfer in cavities. There are many studies on natural

convection in an obstructed cavity in the literatures as (House et al. 1990; Dong and Li, 2004; Braga and Lemos, 2005; Hasanuzzaman et al. 2007; Tasnim and Collins, 2005). Laskowski *et al.* (2007) examined both experimentally and numerically heat transfer to and from a circular cylinder in a cross-flow of water at low Reynolds number. The results explained that, when the lower surface was unheated, the temperatures of the lower surface and water upstream of the cylinder were maintained approximately equal and the flow was laminar. Shih *et al.* (2009) conducted the periodic laminar flow and heat transfer due to an insulated or various isothermal rotating objects (circle, square, and equilateral triangle) placed in the center of the square cavity. Gau and Sharif (2004) conducted mixed convection in rectangular cavities at various aspect ratios with moving isothermal side walls and constant flux heat source on the bottom wall. Gurcan *et al.* (2003) analyzed eddy genesis and transformation of Stokes flow in a double-lid driven cavity. Tsay *et al.* (2003) rigorously investigated the thermal and hydrodynamic interactions among the surface-mounted heated blocks and baffles in a duct flow mixed convection. Bhoite *et al.* (2005) studied numerically the problem of mixed convection flow and heat transfer in a shallow enclosure with a series of block-like heat generating component for a range of Reynolds and Grashof numbers and block-to-fluid thermal conductivity ratios. Gau *et al.* (2000) performed experiments on mixed convection in a horizontal rectangular channel with side heating. Zhou *et al.* (2003) investigated DSC solution for flow in a staggered double-lid driven cavity. Recently, Costa and Raimundo (2010) analyzed the problem of mixed convection in a square enclosure with a rotating cylinder centered within.

The study of MHD mixed convection in lid-driven enclosures has received a continuous attention, due to the interest of the phenomenon in many technological processes. These include design of solar collectors, thermal design of buildings, air conditioning and, recently the cooling of electronic circuit boards. Number of studies on effects of MHD mixed convection in lid-driven cavities is very limited. Chamkha (2003) made a numerical work

on hydromagnetic combined convection flow in a lid-driven cavity with internal heat generation using finite volume approach. The presence of the internal heat generation effects was found to decrease the average Nusselt number significantly for aiding flow and to increase it for opposing flow. Rahman *et al.* (2009) investigated the effect of a heat conducting horizontal circular cylinder on MHD mixed convection in a lid-driven cavity along with joule heating. MHD mixed convection flow in a vertical lid-driven square enclosure, including a heat conducting horizontal circular cylinder with Joule heating was analyzed by Rahman and Alim (2010). The numerical results indicated that the Hartmann number, Reynolds number and Richardson number had strong influence on the streamlines, isotherms, average Nusselt number at the hot wall and average temperature of the fluid in the enclosure. Recently, Rahman *et al.* (2010a) conducted a numerical study on the conjugate effect of joule heating and magneto-hydrodynamics mixed convection in an obstructed lid-driven square cavity, where the developed mathematical model was solved by employing Galerkin weighted residual method of finite element formulation. Rahman *et al.* (2010b) investigated the effect of Reynolds and Prandtl numbers effects on MHD mixed convection in a lid-driven cavity along with joule heating and a centered heat conducting circular block. They showed Buoyancy-induced vortex in the streamlines increased and thermal layer near the cold surface become thin and concentrated with increasing  $Re$ . The influence of Prandtl number on the streamlines in the cavity is found insignificant for all the values of  $Ri$ , whereas the influence of  $Pr$  on the isotherms is remarkable for different values of  $Ri$ . Very recently, Sivasnakan *et al.* (2011) numerically studied the mixed convection in a square cavity of sinusoidal boundary temperatures at the sidewalls in the presence of magnetic field. In their case, the horizontal walls of the cavity are adiabatic. They indicated that the flow behavior and heat transfer rate inside the cavity are strongly affected by the presence of the magnetic field.

To the best knowledge of the authors, no attention has been paid to the problem of MHD mixed convection in a double-lid-driven square cavity with a square heat generating block. The present work focuses on conducting a comprehensive study on the effect of various flow and thermal configurations on MHD mixed convection for a wide range of pertinent controlling parameters in a double-lid-driven square cavity. These parameters include diameter size of the heat-generating block, location of the block in the cavity and Richardson number  $Ri$ .

## 2. PHYSICAL MODEL

The considered two-dimensional model is illustrated in Fig. 1 with boundary conditions and coordinates. The system consists of a double-lid-driven square enclosure with sides of length  $L$ . A heat generating solid square block is placed inside the cavity. In addition, the enclosure is saturated with electrically conducting fluid. The solid block has a thermal conductivity of  $k_s$  and generates

uniform heat flux ( $q$ ) per unit area. Moreover, the vertical walls of the cavity are mechanically lid-driven and considered to be at a constant temperature  $T_c$  and uniform velocity  $V_0$  in the same direction (upward). Besides, the top and bottom surface of the enclosure is kept adiabatic. A transverse magnetic field of strength  $B_0$  is imposed in the normal direction of the double-lids.

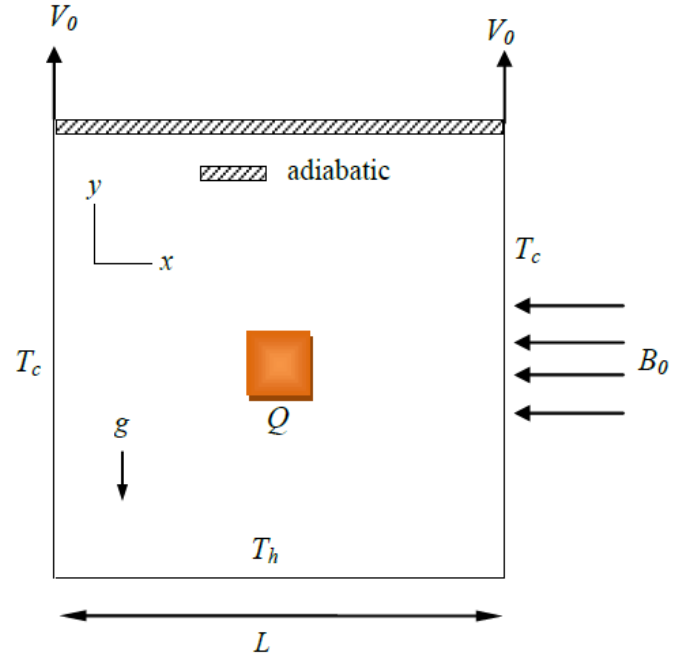


Fig.1. Schematic of the problem

## 3. MATHEMATICAL MODEL

### 3.1 Governing Equations

The system is considered to be a two-dimensional, steady-state, laminar, incompressible, hydromagnetic mixed convection flow inside the enclosure. Newtonian and Boussinesq approximation is applied for fluid with constant physical properties. It is assumed that the radiation and joule heating effect are taken as negligible. The gravitational acceleration acts in the negative  $y$ -direction. The working fluid is assumed to be air ( $Pr = 0.71$ ). Taking into account the above mentioned assumptions the dimensionless governing equations can be obtained via introducing dimensionless variables as follows:

$$X = \frac{x}{L}, Y = \frac{y}{L}, U = \frac{u}{V_0}, V = \frac{v}{V_0}, P = \frac{p}{\rho V_0^2}, \theta = \frac{(T - T_c)}{\Delta T}, \theta_s = \frac{(T_s - T_c)}{\Delta T}$$

Where  $X$  and  $Y$  are the coordinates varying along horizontal and vertical directions respectively,  $U$  and  $V$  are the velocity components in the  $X$  and  $Y$  directions respectively,  $\theta$  is the dimensionless temperature and  $P$  is the dimensionless pressure.

Based on the dimensionless variables above mentioned governing equations (Mass conservation, Momentum and Energy balance equations) can be written as:

$$\frac{\partial U}{\partial X} + \frac{\partial V}{\partial Y} = 0 \quad (1)$$

$$U \frac{\partial U}{\partial X} + V \frac{\partial U}{\partial Y} = -\frac{\partial P}{\partial X} + \frac{1}{Re} \left( \frac{\partial^2 U}{\partial X^2} + \frac{\partial^2 U}{\partial Y^2} \right) \quad (2)$$

$$U \frac{\partial V}{\partial X} + V \frac{\partial V}{\partial Y} = -\frac{\partial P}{\partial Y} + \frac{1}{Re} \left( \frac{\partial^2 V}{\partial X^2} + \frac{\partial^2 V}{\partial Y^2} \right) + Ri \theta - \frac{Ha^2}{Re} V \quad (3)$$

$$U \frac{\partial \theta}{\partial X} + V \frac{\partial \theta}{\partial Y} = \frac{1}{RePr} \left( \frac{\partial^2 \theta}{\partial X^2} + \frac{\partial^2 \theta}{\partial Y^2} \right) \quad (4)$$

For solid block the energy equation is

$$\frac{K}{RePr} \left( \frac{\partial^2 \theta_s}{\partial X^2} + \frac{\partial^2 \theta_s}{\partial Y^2} \right) + Q = 0 \quad (5)$$

where  $Re = \frac{V_0 L}{\nu}$ ,  $Pr = \frac{\nu}{\alpha}$ , and  $Ri = \frac{g \beta \Delta T L}{V_0^2}$  are Reynolds number, Prandtl number and Richardson number, respectively and  $Q = \frac{q L^2}{k_s \Delta T}$  is the heat generating parameter in the solid block

( $\Delta T = T_b - T_c$  and  $\alpha = k/\rho C_p$  are the temperature difference and thermal diffusivity respectively). Here  $Ha$  is Hartmann number which is defined as  $Ha^2 = \frac{\sigma B_0^2 L^2}{\mu}$ .

### 3.2 Boundary conditions

The physical boundary conditions are illustrated in the physical model (Fig. 1). The boundary conditions for the present problem are specified as follows:

At sliding double-lids:  $U = 0, V = 1, \theta = 0$

At horizontal top and bottom wall:

$$U = V = 0, \quad \frac{\partial \theta}{\partial N} = 0$$

At square block boundaries:  $U = V = 0, \theta = \theta_b$

$$\text{At fluid-solid interface: } \left( \frac{\partial \theta}{\partial N} \right)_{fluid} = K \left( \frac{\partial \theta_s}{\partial N} \right)_{solid}$$

Where  $N$  is the non-dimensional distances either  $X$  or  $Y$  direction acting normal to the surface and  $K$  is the ratio of solid fluid thermal conductivity ( $k_s/k$ ).

Expanding the velocity components ( $U, V$ ) and temperature ( $\theta$ ) using basis set  $\{\Phi_k\}_{k=1}^N$  as

$$U \approx \sum_{k=1}^N U_k \Phi_k(X, Y), \quad V \approx \sum_{k=1}^N V_k \Phi_k(X, Y), \quad \theta \approx \sum_{k=1}^N \theta_k \Phi_k(X, Y), \text{ and } \theta_s \approx \sum_{k=1}^N \theta_{s,k} \Phi_k(X, Y) \quad (9)$$

### 3.3 Heat Transfer Calculation

The average Nusselt number  $Nu$  along a surface  $S$  of the block may be calculated as follows:

$$Nu_{av} = -\frac{1}{L_s} \int_0^{L_s} \frac{\partial \theta}{\partial n} dS$$

where  $L_s$  is the length of heated surface of the block and  $n$  represents the unit normal vector on the surface of the solid block.

The average temperature of the fluid is defined as:

$$\theta_{av} = \int \theta d\bar{V} / \bar{V}$$

where  $n$  represents the unit normal vector on the surface of the solid body and  $\bar{V}$  is the cavity volume.

## 4. NUMERICAL SCHEME

To solve the governing equations along with the boundary conditions, the Galerkin weighted residual finite element techniques are used. The formulation of this method and computational procedure are discussed in the following two sections:

### 4.1 Finite element formulation and computational process

Galerkin finite element method is discussed to solve the non-dimensional governing equations along with boundary conditions for the present problem. The equation of continuity (Eq. (1)) is used as a constraint due to mass conservation and this restriction can be used to compute the pressure distribution. To solve equations (2) - (5), the Penalty finite element method (More detailed in (Roy and Basak, 2005; Saha, 2010) is performed where the pressure  $P$  is eliminated by a penalty constraint  $\gamma$  and the incompressibility criteria given by Eq. (1) consequences in

$$P = -\gamma \left( \frac{\partial U}{\partial X} + \frac{\partial V}{\partial Y} \right) \quad (6)$$

The continuity equation is automatically fulfilled for large values of  $\gamma$ . Using Eq. (6) the momentum equations (2 - 3) become:

$$U \frac{\partial U}{\partial X} + V \frac{\partial U}{\partial Y} = \gamma \frac{\partial}{\partial X} \left( \frac{\partial U}{\partial X} + \frac{\partial V}{\partial Y} \right) + \frac{1}{Re} \left( \frac{\partial^2 U}{\partial X^2} + \frac{\partial^2 U}{\partial Y^2} \right) \quad (7)$$

$$U \frac{\partial V}{\partial X} + V \frac{\partial V}{\partial Y} = \gamma \frac{\partial}{\partial Y} \left( \frac{\partial U}{\partial X} + \frac{\partial V}{\partial Y} \right) + \frac{1}{Re} \left( \frac{\partial^2 V}{\partial X^2} + \frac{\partial^2 V}{\partial Y^2} \right) + Ri \theta - \frac{Ha^2}{Re} V \quad (8)$$

Then the Galerkin finite element method yields the following nonlinear residual equations for the Eqs. (4), (5), (7), and (8) respectively at nodes of internal domain A:

$$R_i^{(1)} = \sum_{k=1}^N \theta_k \int_A \left[ \left( \sum_{k=1}^N U_k \Phi_k \right) \frac{\partial \Phi_k}{\partial X} + \left( \sum_{k=1}^N V_k \Phi_k \right) \frac{\partial \Phi_k}{\partial Y} \right] \Phi_i dXdY - \frac{1}{Re Pr} \sum_{k=1}^N \theta_k \int_A \left[ \frac{\partial \Phi_i}{\partial X} \frac{\partial \Phi_k}{\partial X} + \frac{\partial \Phi_i}{\partial Y} \frac{\partial \Phi_k}{\partial Y} \right] dXdY \quad (10)$$

$$R_i^{(4)} = \sum_{k=1}^N V_k \int_A \left[ \left( \sum_{k=1}^N U_k \Phi_k \right) \frac{\partial \Phi_k}{\partial X} + \left( \sum_{k=1}^N V_k \Phi_k \right) \frac{\partial \Phi_k}{\partial Y} \right] \Phi_i dXdY - \gamma \left[ \sum_{k=1}^N U_k \int_A \frac{\partial \Phi_i}{\partial Y} \frac{\partial \Phi_k}{\partial X} dXdY + \sum_{k=1}^N V_k \int_A \frac{\partial \Phi_i}{\partial Y} \frac{\partial \Phi_k}{\partial Y} dXdY \right] - \frac{1}{Re} \sum_{k=1}^N V_k \int_A \left[ \frac{\partial \Phi_i}{\partial X} \frac{\partial \Phi_k}{\partial X} + \frac{\partial \Phi_i}{\partial Y} \frac{\partial \Phi_k}{\partial Y} \right] dXdY - Ri \int_A \left( \sum_{k=1}^N \theta_k \Phi_k \right) \Phi_i dXdY + \frac{Ha^2}{Re} \int_A \left( \sum_{k=1}^N V_k \Phi_k \right) \Phi_i dXdY \quad (13)$$

Three points Gaussian quadrature is used to evaluate the integrals in the residual equations. The non-linear residual equations (10 – 13) are solved using Newton–Raphson method to determine the coefficients of the expansions in Eq. (9).

To solve the sets of the global nonlinear algebraic equations in the form of a matrix, the Newton-Raphson iteration technique has been adapted. The convergence of solutions is assumed when the relative error for each variable between consecutive iterations is recorded below the convergence criterion  $\epsilon$  such that  $|\Psi^{n+1} - \Psi^n| \leq 10^{-4}$ ,  $n$  is number of iteration and  $\Psi$  is a function of  $U, V, \theta$  and  $\theta_s$ .

#### 4.2 Grid refinement check and Code Validation

In order to obtain grid independent solution, a grid sensitivity test is performed for a square lid-driven cavity to choose the proper grid for the numerical simulation. In the present study, the solution domain is divided into a set of non-overlapping regions called elements. Non-uniform triangular element grid system is employed here. Five different non-uniform grid systems with the following number of elements within the resolution field: 4032, 4794, 6116, 6220 and 7744 are examined in this study. In addition, the numerical scheme is employed for highly precise key in the average Nusselt  $Nu$  number for the aforesaid elements to develop an understanding of the grid fineness as shown in Fig. 2. The scale of average Nusselt number for 6220 elements shows a very little difference with the results obtained for the other elements. Hence considering the non-uniform grid system of 6220 elements is preferred for the computation of all cases. The validity of the code is available in Rahman *et al.* (2010a) and is not repeated here.

$$R_i^{(2)} = \frac{K}{Re Pr} \sum_{k=1}^N \theta_{s,k} \int_A \left[ \frac{\partial \Phi_i}{\partial X} \frac{\partial \Phi_k}{\partial X} + \frac{\partial \Phi_i}{\partial Y} \frac{\partial \Phi_k}{\partial Y} \right] dXdY + Q \quad (11)$$

$$R_i^{(3)} = \sum_{k=1}^N U_k \int_A \left[ \left( \sum_{k=1}^N U_k \Phi_k \right) \frac{\partial \Phi_k}{\partial X} + \left( \sum_{k=1}^N V_k \Phi_k \right) \frac{\partial \Phi_k}{\partial Y} \right] \Phi_i dXdY - \gamma \left[ \sum_{k=1}^N U_k \int_A \frac{\partial \Phi_i}{\partial X} \frac{\partial \Phi_k}{\partial X} dXdY + \sum_{k=1}^N V_k \int_A \frac{\partial \Phi_i}{\partial X} \frac{\partial \Phi_k}{\partial Y} dXdY \right] - \frac{1}{Re} \sum_{k=1}^N U_k \int_A \left[ \frac{\partial \Phi_i}{\partial X} \frac{\partial \Phi_k}{\partial X} + \frac{\partial \Phi_i}{\partial Y} \frac{\partial \Phi_k}{\partial Y} \right] dXdY \quad (12)$$

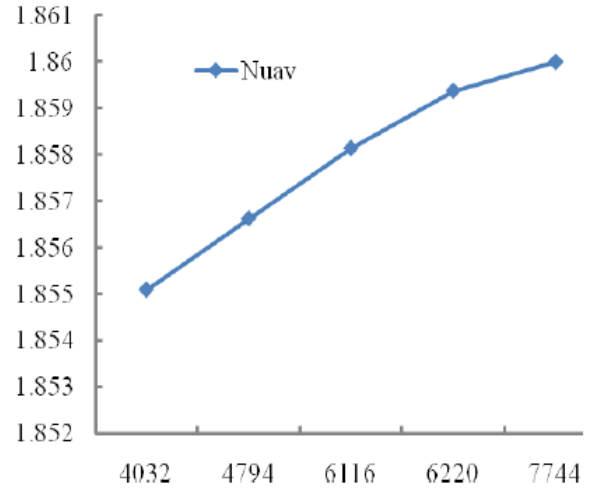


Fig. 2. Effect of grid refinement test on average Nusselt number  $Nu$ , while  $Q = 1.0$   $Ri = 10.0$  and  $Ha = 10.0$ .

## 5. RESULTS AND DISCUSSION

MHD mixed convection inside a lid driven cavity having a heat-generating square block is governed by eight controlling parameters. These parameters are Hartmann number  $Ha$ , heat generation  $Q$ , solid fluid thermal conductivity ratio  $K$ , Reynolds number  $Re$ , Prandtl number  $Pr$  heat-generating block diameter  $D$ , location of the block in the cavity and Richardson number  $Ri$ . Investigation of the present study is made for three parameters namely, heat-generating block diameter  $D$ , location of the block in the cavity and  $Ri$ , which influence the flow fields and temperature distribution inside the cavity. The parameters  $D$  and  $Ri$  are varied in the ranges of 0.1-0.4, and 0.0-10.0, respectively, while the other parameters  $Re, Ha, K$  and  $Pr$

are fixed at 100, 20, 5.0 and 0.71, in that order. The computation is performed for pure forced convection ( $Ri=0.0$ ), pure mixed convection ( $Ri=1.0$ ), and dominant natural convection ( $Ri=10.0$ ). We presented the results of this current study in three sections. The first section will focus on flow structure, which contains streamlines for mentioned cases. The second section deals with the temperature field in terms of isotherms. The final section will discuss heat transfer including variation of average Nusselt number  $Nu$  and the dimensionless average bulk temperature  $\theta_{av}$  the temperature  $\theta_c$  at the block centre.

### 5.1 Flow Structure

The characteristics of the flow field in the lid driven cavity is examined by exploring the effects of Richardson numbers, block size as well as position of the block in the cavity. The effect of block size (placed at the center of the cavity) on the flow fields as streamlines in a square cavity operating at three different values of  $Ri$ , while the values of  $K$ ,  $Re$ ,  $Ha$ ,  $Pr$ , and  $Q$  are keeping fixed at 5.0, 100, 10.0, 0.71 and 1.0, respectively, are presented in the Fig. 3. From this figure, it is clearly seen that the forced convection plays a dominant role and the recirculation flow is mostly generated only by the moving lids at low  $Ri$  ( $= 0.0$ ) and  $D$  ( $= 0.1$ ). The recirculation flow rotates in the clockwise (CW) and counter clockwise (CCW) direction near the left and right vertical wall, respectively, which is expected since the lids are moving upwards. Further at low  $Ri$  ( $= 0.0$ ) and for the higher values of  $D$  ( $= 0.2, 0.3$  and  $0.4$ ), the flow patterns inside the cavity remain unchanged except the shape and position of the core of the circulatory flow. As the value of  $D$  increases the core vortices expand vertically.

It indicates the reduction of the flow strength of those vortices. Next at  $Ri = 1.0$ , a pair of counter rotating cells appear in the flow domain for the lower values of  $D$  ( $= 0.1, 0.2$  and  $0.3$ ), whereas the fluid flow is characterized by a clockwise and a counter clockwise rotating vortex generated by the movement of the vertical walls. But four small vortices are added between the CW and a CCW rotating cells inside the cavity for the highest value of  $D$  ( $= 0.4$ ). This behavior is very logical because the large cylinder reduces the available space for the buoyancy-induced recirculation. Further at  $Ri = 10.0$ , which is a buoyancy dominated regime, two pair of vortices appear between the block and vertical lids for all  $D$ . It is clearly observed that the size and the shape of the core of the vortices near the block expand gradually with the increasing  $D$ -values as a result the size and the shape of the core of the vortices near the vertical lids reduces for the space constraint.

The dependence of flow fields on the locations of the block can be observed in the plots of streamlines for the various values of the Richardson number from Fig. 4, while  $AR = 1.0$ ,  $Re = 100$ ,  $Ha = 10.0$ ,  $Q = 1.0$ ,  $D = 0.2$ ,  $Pr = 0.71$  and  $K = 5.0$  are kept fixed. From the bottom row of this figure, it is seen that in the pure forced and mixed convection region ( $Ri = 0.0$  and  $Ri = 1.0$ ) the flow patterns

inside the cavity remain unchanged at the same locations of the block, except the shape of the core of the circulatory flow which is expected. However, in the free convection dominated region ( $Ri = 10.0$ ) it is seen from the right column that the number of recirculation cells increase comparing with the flow pattern of  $Ri = 1.0$ . When the inner block moves closer to the right vertical wall along the mid-horizontal plane a reversed result is observed as it compared to the previous position. Furthermore at  $Ri= 0.0$  and  $1.0$ , when the heat generating block moves near the bottom insulated wall of the cavity along the mid vertical plane, then two pair of counter rotating vortices are formed in the cavity near the vertical lids. It is noticed that the tendency of the core of vortices expand to the upper part of the cavity along the vertical lids. But, while the inner block moves closer to the upper horizontal wall along the mid-vertical plane an opposite result is found as it compared to the earlier location. It is also seen that the number of eddies increased for higher value of  $Ri$  ( $=10.0$ ) for every location of the heat-generating block.

### 5.2 Thermal Field

The characteristics of thermal field in the lid driven cavity is analyzed by plotting the effects of Richardson numbers, block size as well as location of the block in the cavity. The corresponding effect of the size of the heat-generating block on thermal fields as isotherms at various values of  $Ri$  shown in the Fig. 5. We can ascertain that for  $Ri = 0.0$  and  $D = 0.0$ , the parabolic shape isotherms are observed near the hot surface and the number of open isothermal lines escalating with the rising values of  $D$ . Furthermore, similar trend is observed in the isotherms for different values of  $D$  at  $Ri = 1.0$ , which is due to the conjugate effect of conduction and mixed convection flow in the cavity. From the left and middle columns of Fig. 5, one may notice that the isotherm pattern seems to be like the upper human torso for lower values  $D$  ( $= 0.2$  and  $0.3$ ). As  $Ri$  increases further from 1.0 to 10.0, the shape of thermal layer is just upturned from forced and mixed convection regions ( $Ri = 0.0$  and  $1.0$ ) for higher values of  $D$  ( $= 0.2, 0.3, 0.4$ ) values of, which is owing to the strong influence of the convective current in the cavity.

The influence of the thermal fields on the locations of the heat-generating block in the cavity can be obtained in the plots of the isotherms for various values of the block locations in Fig. 6, while  $AR = 1.0$ ,  $Re = 100$ ,  $Ha = 10.0$ ,  $Q = 1.0$ ,  $D = 0.2$ ,  $Pr = 0.71$  and  $K = 5.0$  are kept fixed. At  $Ri = 0.0$  and different locations of the block, the isothermal lines near the heat source are parallel to the nearest vertical wall due to the dominating influence of the conduction and mixed convection heat transfer. One may notice that higher values isotherms seem to be elliptic rounding the heat-generating block. A similar development is observed for  $Ri = 1.0$ . On the other hand, the shape of thermal layer for  $Ri = 10.0$  is just reversed from forced and mixed convection regions for all considered locations of the heat-generating body.

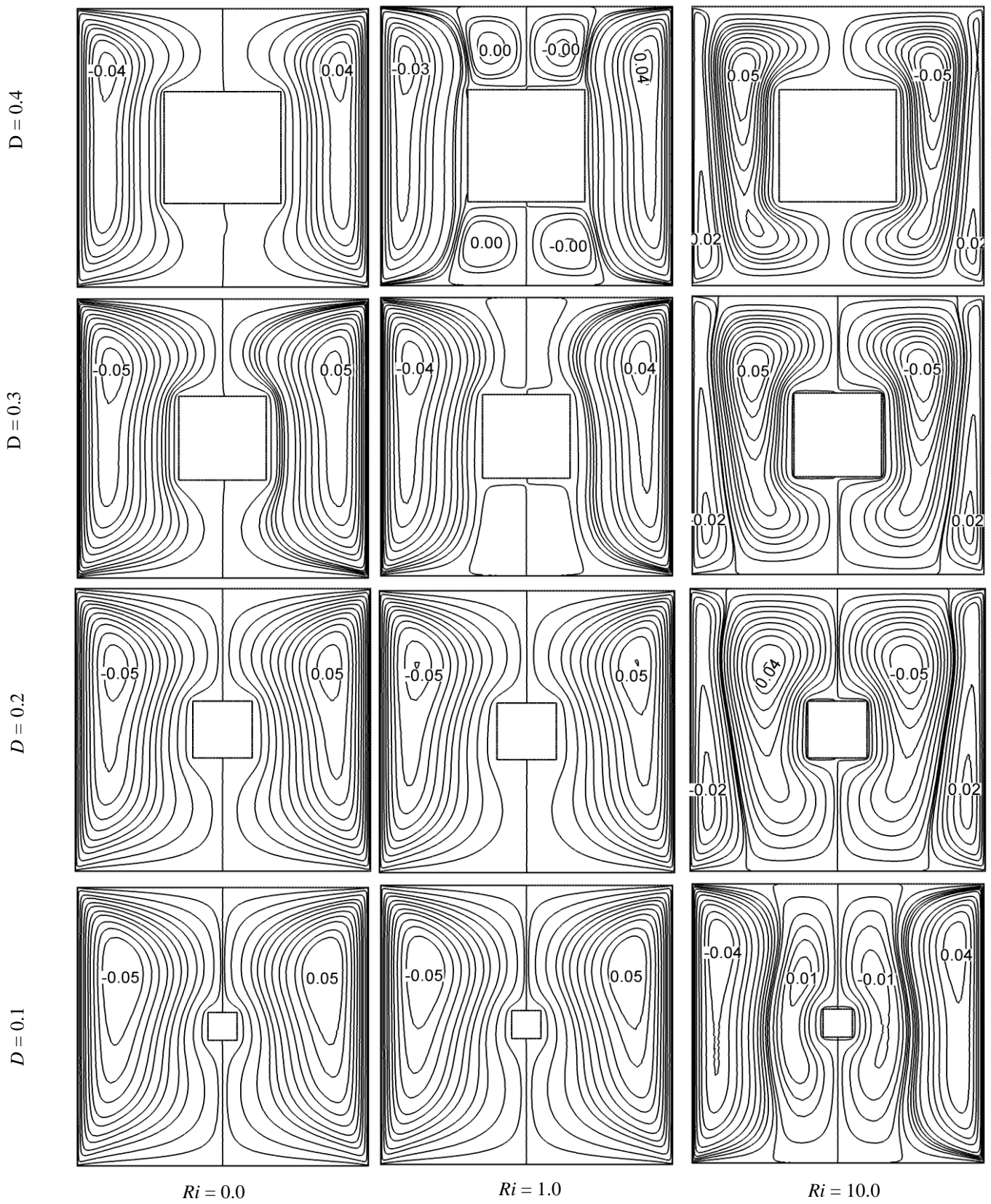


Fig. 3: Streamlines for different values of cylinder size  $D$  and Richardson number  $Ri$ , while  $AR = 1.0$ ,  $Ha = 10.0$ ,  $Q = 1.0$ ,  $Pr = 5.0$ ,  $K = 5.0$ ,  $Re = 100$  and  $(L_x, L_y) = (0.5, 0.5)$ .

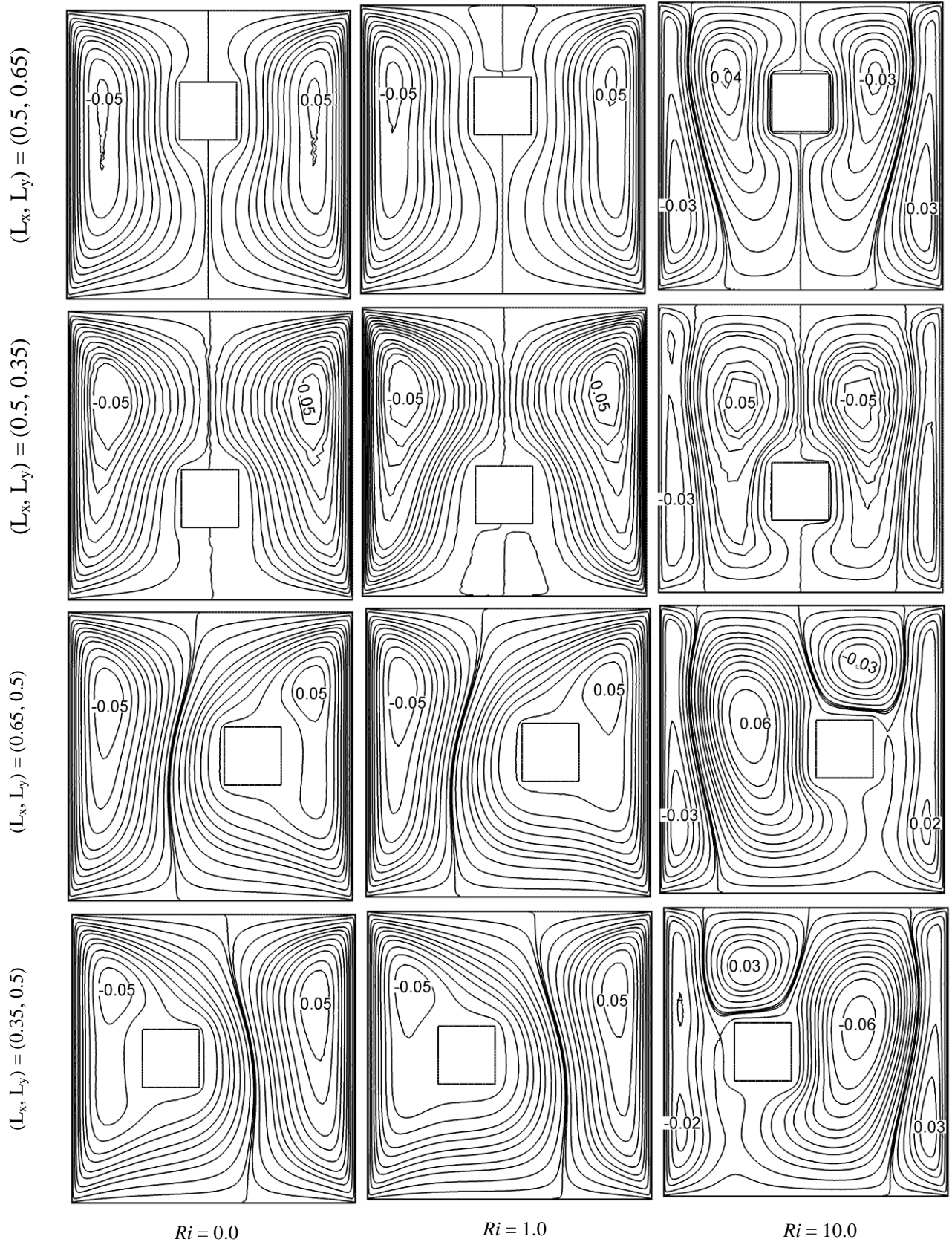


Fig. 4: Streamlines for different values of cylinder locations  $(L_x, L_y)$  and Richardson number  $Ri$ , while  $AR = 1.0$ ,  $D = 0.2$ ,  $Ha = 10.0$ ,  $Q = 1.0$ ,  $Pr = 5.0$ ,  $K = 5.0$  and  $Re = 100$ .

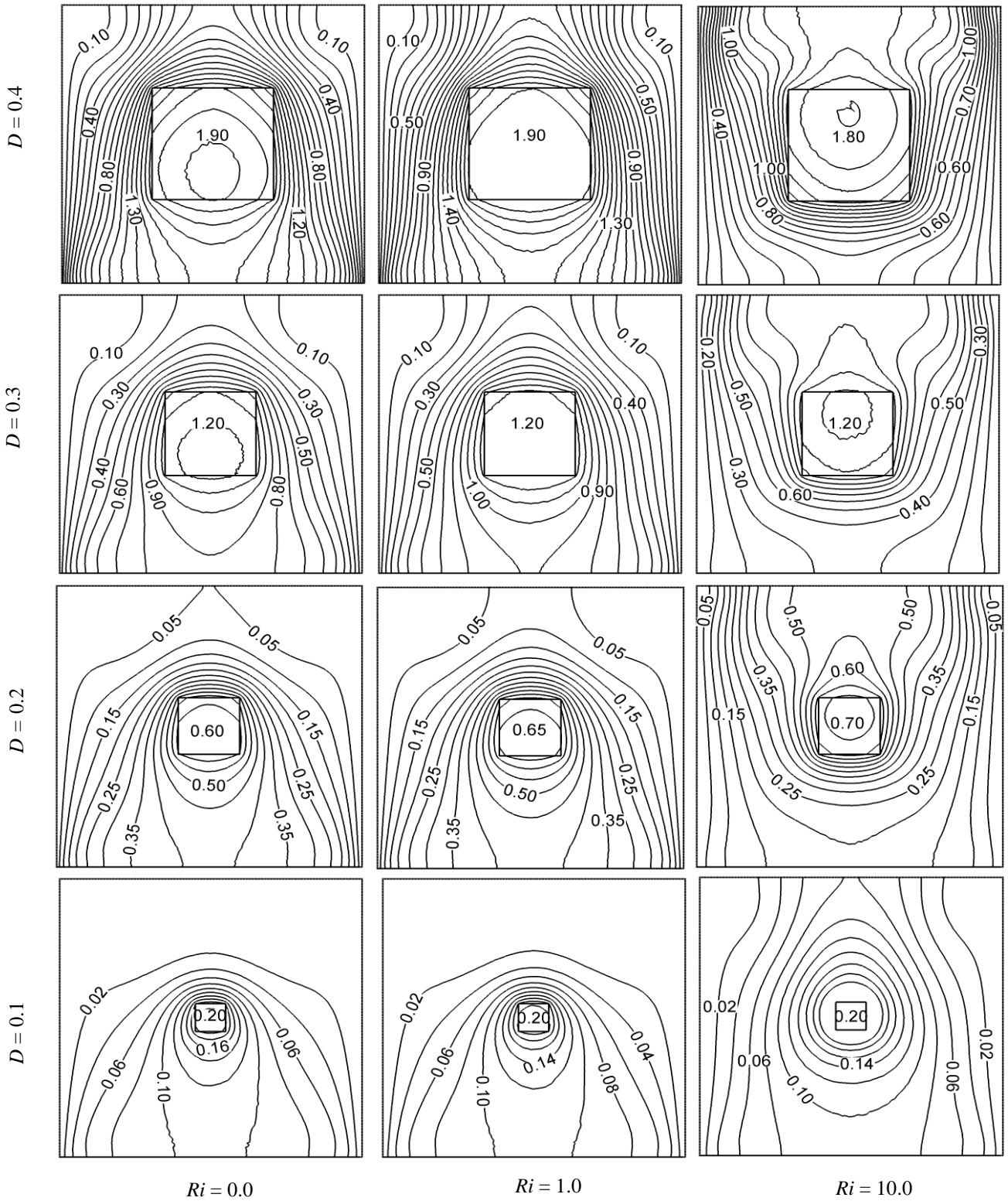


Fig. 5: Isotherms for different values of cylinder size  $D$  and Richardson number  $Ri$ , while  $AR = 1.0$ ,  $Ha = 10.0$ ,  $Q = 1.0$ ,  $Pr = 5.0$ ,  $K = 5.0$ ,  $Re = 100$  and  $(L_x, L_y) = (0.5, 0.5)$ .

### 5.3 Heat Transfer

The variation of the average Nusselt number at the heated surface, average temperature  $\theta_{av}$  of the fluid in the cavity and temperature  $\theta_c$  at the block center

against  $Ri$  at various values of  $D$  is shown in the Fig. 7. It is observed from the bottom figure that the heat transfer rate  $Nu$  decreases very slowly with the rising value of  $Ri$  for the higher values of  $D$  ( $= 0.2, 0.3$ , and  $0.4$ ). But  $Nu$  remains unaltered for the lowest value

of  $D$  for the considered  $Ri$ . It is to be highlighted here that maximum heat transfer rate occurs for largest value of  $D$  ( $= 0.4$ ). On the other hand,  $\theta_{av}$  and  $\theta_c$  at the block center increase with the increasing  $Ri$  upto 2.5 then it declined for the higher values of  $D$  ( $= 0.2, 0.3, \text{ and } 0.4$ ). But  $\theta_{av}$  and  $\theta_c$  are unaffected for the lowest value of  $D$  for all values of  $Ri$ . The average Nusselt number at the heated surface, average fluid temperature  $\theta_{av}$  in the cavity and the temperature  $\theta_c$  at the block center are plotted against Richardson numbers in Fig. 8 for the four different locations of the

heat-generating body. For each locations of the block, the  $Nu-Ri$  profile is parabolic shape shows two distinct zones depending on Richardson number. Up to a certain value of  $Ri$  the distribution of  $Nu$  smoothly decreases with increasing  $Ri$  and beyond these values of  $Ri$  it increases with  $Ri$ . On the other hand, average fluid temperature  $\theta_{av}$  in the cavity and the temperature  $\theta_c$  at the block center increase monotonically with  $Ri$  (up to a certain value of  $Ri$ ) and the decreasing at each locations of the cylinder except the location  $L_x=0.35, L_y=0.50$ .

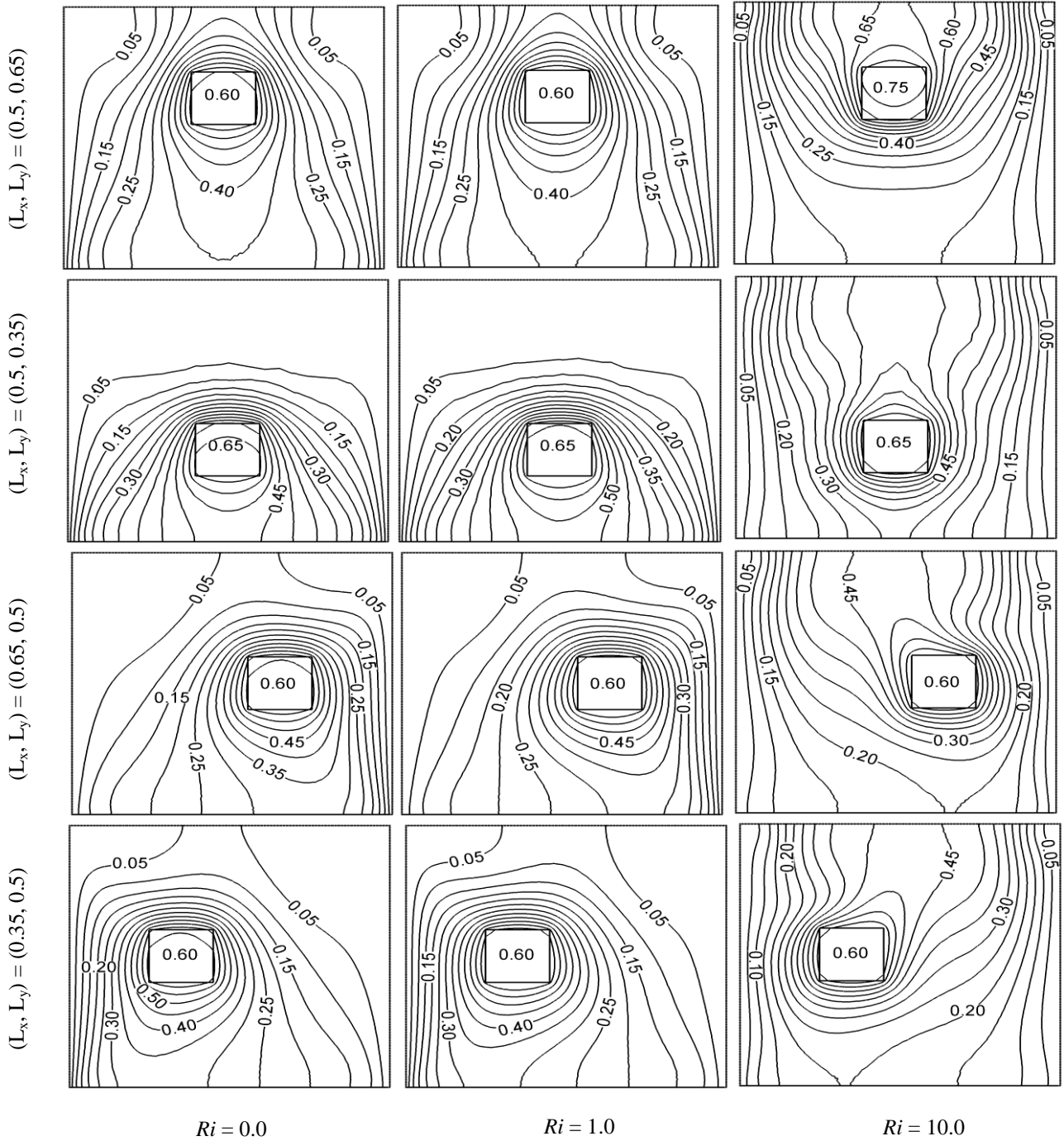


Fig. 6: Isotherms for different values of cylinder locations ( $L_x, L_y$ ) and Richardson number  $Ri$ , while  $AR = 1.0, D = 0.2, Ha = 10.0, Q = 1.0, Pr = 5.0, K = 5.0$  and  $Re = 100$ .

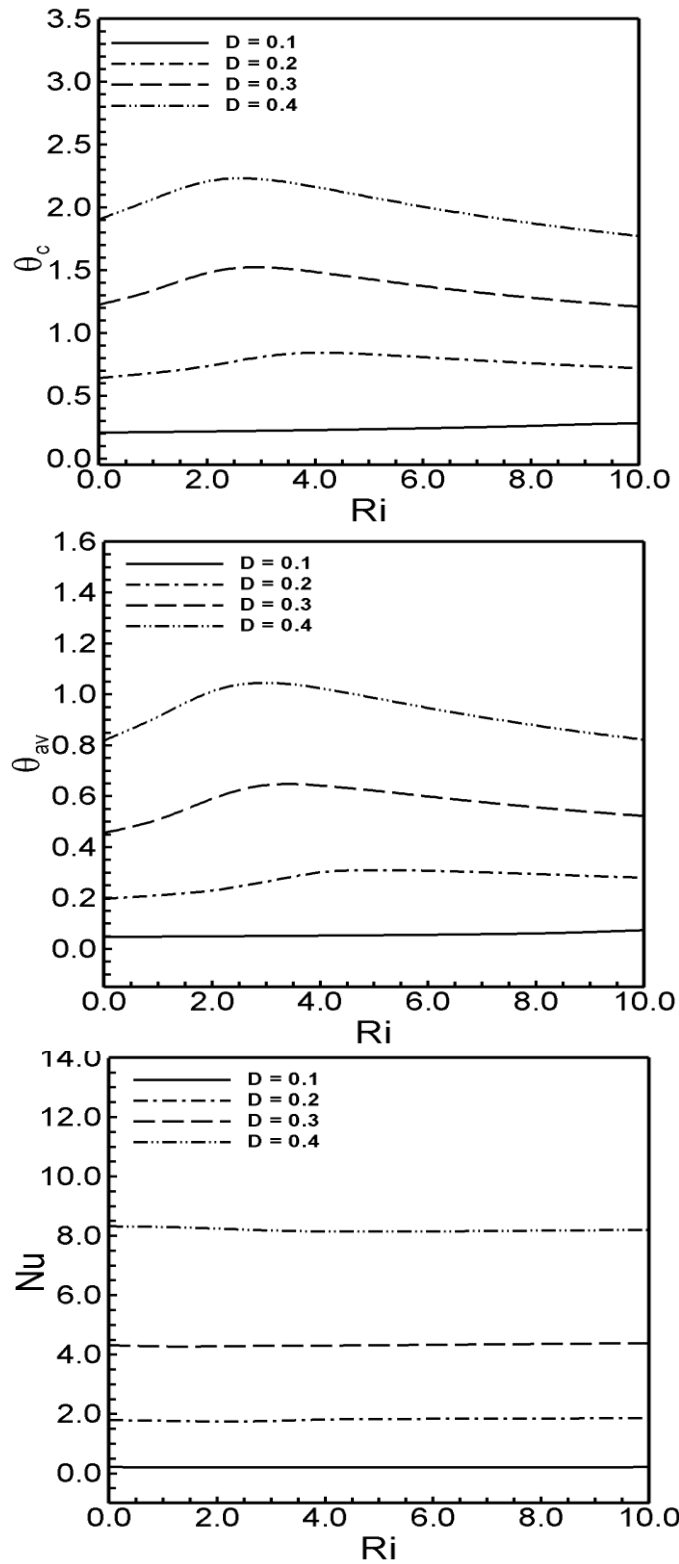


Fig 7: Effect of cylinder size  $D$  on (i) average Nusselt number, (ii) average fluid temperature and (ii) temperature at the cylinder centre, while  $AR = 1.0$ ,  $Ha = 10.0$ ,  $Q = 1.0$ ,  $Pr = 5.0$ ,  $K = 5.0$ ,  $Re = 100$  and  $(L_x, L_y) = (0.5, 0.5)$ .

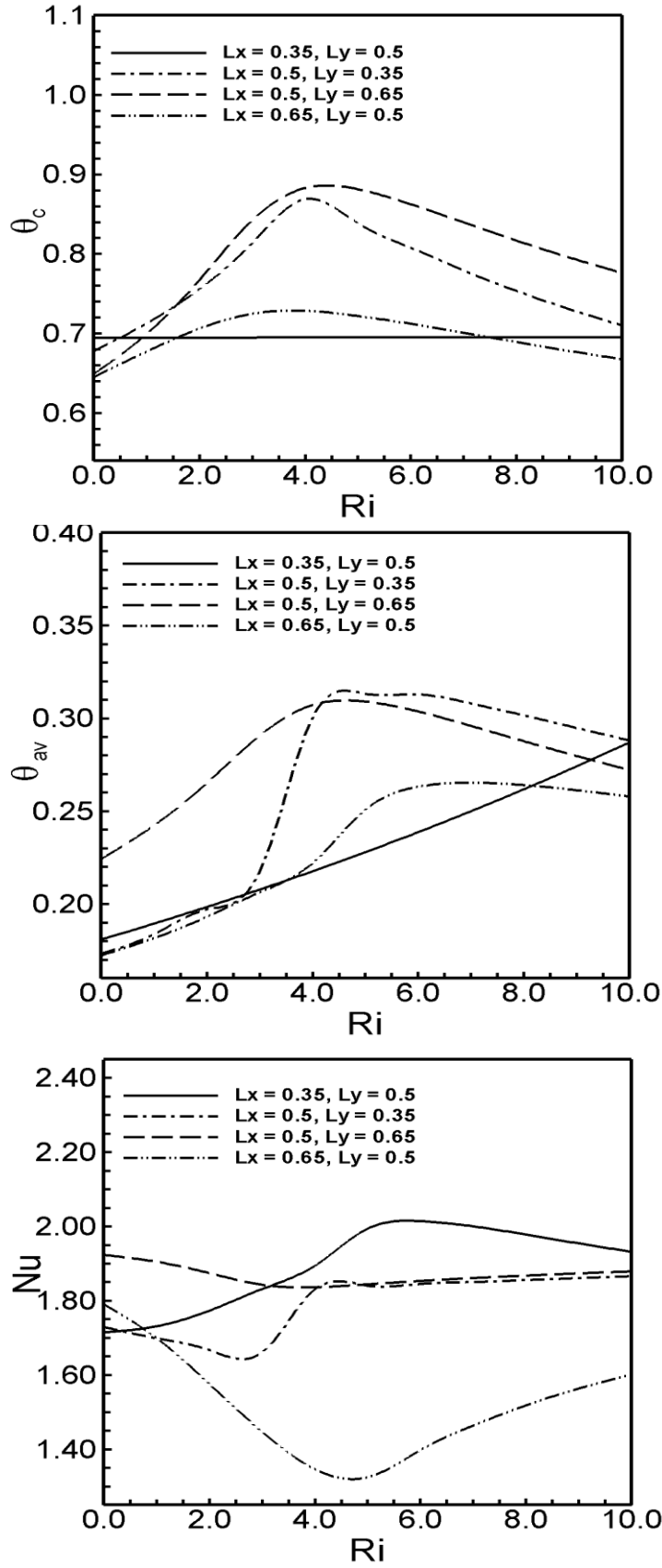


Fig. 8: Effect of cylinder locations ( $L_x, L_y$ ) on (i) average Nusselt number, (ii) average fluid temperature and (ii) temperature at the cylinder centre, while  $AR = 1.0, D = 0.2, Ha = 10.0, Q = 1.0, Pr = 5.0, K = 5.0$  and  $Re = 100$ .

## 6. CONCLUSION

A computational study is performed to investigate the MHD mixed convection flow in a double-lid driven enclosure with a heat-generating horizontal square block. Results are obtained for wide ranges of heat-generating block diameter  $D$  and the location of the block in the cavity. The following conclusions may be drawn from the present investigations:

- The heat-generating block size has a significant influence on the flow and thermal fields in the cavity. Higher average Nusselt number is always found for the largest value of  $D$  for three convective regimes. The average temperature of the fluid and temperature at the cylinder center in the cavity are lesser for  $D = 0.1$ .
- It is observed that the location of the block is one of the most important parameter on fluid flow, temperature fields and heat transfer characteristics. Moreover, noticeably different flow behaviors and heat transfer characteristics are observed among the three different flow regimes. The value of the average Nusselt number is greater if the heat-generating cylinder is placed near the left wall along the mid-horizontal plane at  $Ri > 2.5$  and beyond these values of  $Ri$  it is the highest when the cylinder moves near the bottom insulated wall of the cavity along the mid vertical plane.

## ACKNOWLEDGEMENT

The authors like to express their gratitude to the Committee for Advanced Studies & Research Directorate of Advisory Extension & Research Services, Bangladesh University of Engineering and Technology (BUET).

## NOMENCLATURES

$B_o$	Magnetic field strength
$C_p$	Specific heat of fluid at constant pressure
$D$	Block diameter ( $m$ )
$g$	Gravitational acceleration ( $ms^{-2}$ )
$Ha$	Hartmann number
$k$	Thermal conductivity of fluid ( $Wm^{-1}K^{-1}$ )
$k_s$	Thermal conductivity of solid ( $Wm^{-1}K^{-1}$ )
$K$	Thermal conductivity ratio of the solid and fluid
$L$	Length of the cavity ( $m$ )
$Nu$	Nusselt number
$p$	Dimensional pressure ( $Nm^{-2}$ )

$P$	Non-dimensional pressure
$Pr$	Prandtl number
$q$	Heat generation per unit volume of the block ( $W/m^3$ )
$Q$	Heat generating parameter
$Re$	Reynolds number
$Ri$	Richardson number
$T$	Dimensional temperature (K)
$u, v$	Velocity components ( $ms^{-1}$ )
$U, V$	Non-dimensional velocity components,
$\bar{V}$	Cavity volume ( $m^3$ )
$x, y$	Cartesian coordinates ( $m$ )
$X, Y$	Non-dimensional Cartesian coordinates

## Greek symbols

$\alpha$	Thermal diffusivity ( $m^2s^{-1}$ )
$\beta$	Thermal expansion coefficient ( $K^{-1}$ )
$\nu$	Kinematic viscosity of the fluid ( $m^2s^{-1}$ )
$\theta$	Non-dimensional temperature
$\rho$	Density of the fluid ( $Kg m^{-3}$ )

## Subscripts

$av$	Average
$b$	Block surface
$c$	Less heated wall
$h$	Heated wall
$s$	Solid

## REFERENCES

- Al-Amiri, A., Khanafer, K., Bull, J., Pop, I. 2007. Effect of sinusoidal wavy bottom surface on mixed convection heat transfer in a lid-driven cavity, *Int. J. of Heat and Mass Transfer*, 50, 1771-1780
- Bhoite, M.T., Narasimham, G.S.V.L., Murthy, M.V.K. 2005. Mixed convection in a shallow enclosure with a series of heat generating components, *Int. J. of Thermal Sciences*, 44, 125-135.
- Braga, E.J., de Lemos, M.J.S. 2005. Laminar natural convection in cavities filled with circular and square rods, *Int. Commun. Heat and Mass Transfer*, 32, 1289-1297.
- Chamkha, A. J. 2003. Hydromagnetic combined convection flow in a vertical lid-driven cavity with

- internal heat generation or absorption, Numer. Heat Transfer, Part A, 41, 529-546.
- Costa, V. A. F., Raimundo, A. M. 2010. Steady mixed convection in a differentially heated square enclosure with an active rotating circular cylinder, Int. J. of Heat and Mass Transfer, 53, 1208-1219.
- Dong, S.F., Li, Y.T. 2004. Conjugate of natural convection and conduction in a complicated enclosure, Int. J. of Heat and Mass Transfer, 47, 2233-2239.
- Gau, C., Jeng, Y.C., Liu, C.G., 2000. An experimental study on mixed convection in a horizontal rectangular channel heated from a side", ASME J. Heat Transfer, 122, 701-707.
- Gau, G., Sharif, M.A.R. 2004. Mixed convection in rectangular cavities at various aspect ratios with moving isothermal side walls and constant flux heat source on the bottom wall, Int. J. of Thermal Sciences, 43, 465-475.
- Gu'rcan, F., Gaskell, P.H., Savage, M.D., Wilson, M C T. 2003. Eddy genesis and transformation of Stokes flow in a double-lid driven cavity, Proc. Instn Mech. Engrs Vol. 217 Part C: J. Mechanical Engineering Science, 353-364.
- Hasanuzzaman, M., Saidur, R., Ali, M., Masjuki, H.H. 2007. Effects of variables on natural convective heat transfer through V-corrugated vertical plates, International Journal of Mechanical and Materials Engineering, 2(2), 109-117
- Hasanuzzaman, M., Saidur, R., Masjuki, H. H. 2009. Effects of operating variables on heat transfer, energy losses and energy consumption of household refrigerator-freezer during the closed door operation, Energy, 34(2), 196-198.
- House, J. M. Beckermann, C., Smith, T. F. 1990. Effect of a centered conducting body on natural convection heat transfer in an enclosure, Numer. Heat Transfer, Part A, 18, 213-225.
- Hsu, T. H., How, S. P. 1999. Mixed convection in an enclosure with a heat-conducting body, Acta Mechanica, 133, 87-104.
- Laskowski, G., Kearney, S., Evans, G., Greif, R. 2007. Mixed convection heat transfer to and from a horizontal cylinder in cross-flow with heating from below, Int. J. of Heat and Fluid Flow, 28, 454-468.
- Manca, O., Nardini, S., Khanafer, K., Vafai, K. 2003. Effect of Heated Wall Position on Mixed Convection in a Channel with an Open Cavity, Numer. Heat Transfer, Part A, 43, 259-282.
- Omri, A., Nasrallah, S. B. 1999. Control Volume Finite Element Numerical Simulation of Mixed Convection in an Air-Cooled Cavity, Numer. Heat Transfer, Part A, 36, 615-637.
- Rahman, M.M., Alim, M.A. 2010. MHD mixed convection flow in a vertical lid-driven square enclosure including a heat conducting horizontal circular cylinder with Joule heating, Nonlinear Analysis: Modelling and Control, 15 (2), 199-211.
- Rahman, M.M., Alim, M.A., Sarker, M.M.A. 2010. Numerical study on the conjugate effect of joule heating and magneto-hydrodynamics mixed convection in an obstructed lid-driven square cavity, Int. Commun. Heat and Mass Transfer, 37 (5), 524-534.
- Rahman, M.M., Billah, M. M., Mamun, M. A. H., Saidur, R., Hassanuzzaman, M. 2010 Reynolds and Prandtl numbers effects on MHD mixed convection in a lid-driven cavity along with joule heating and a centered heat conducting circular block, International Journal of Mechanical and Materials Engineering, 5 (2), 163-170.
- Rahman, M.M., Mamun, M.A.H., Saidur, R., Nagata, S. 2009. Effect of a heat conducting horizontal circular cylinder on MHD mixed convection in a lid-driven cavity along with joule heating, International Journal of Mechanical and Materials Engineering, 4 (3), 256-265.
- Roy, S., Basak, T. 2005. Finite element analysis of natural convection flows in a square cavity with nonuniformly heated wall(s), Int. J. Eng. Sci. 43, 668-680.
- Saha, G. 2010. Finite element simulation of magnetoconvection inside a sinusoidal corrugated enclosure with discrete isoflux heating from below, Int. Commun. Heat and Mass Transfer, 37, 393-400.
- Shih, Y., Khodadadi, J., Weng, K., Ahmed, A. 2009. Periodic fluid flow and heat transfer in a square cavity due to an insulated or isothermal rotating cylinder, J. of Heat Transfer, 131, 1-11.
- Shokouhmand, H., Sayehvand, H. 2004. Numerical study of flow and heat transfer in a square driven cavity, Int. J. of Engg., Transactions A: Basics 17 (3), 301-317.
- Sivasankaran, S., Malleswaran, A., Lee, J., Sundar, P. 2011. Hydro-magnetic combined convection in a lid-riven cavity with sinusoidal boundary conditions on both sidewalls, Int. J. Heat Mass Transfer, 54, 512-525.
- Tasnim, S.H., Collins, M.R. 2005. Suppressing natural convection in a differentially heated square cavity with an arc shaped baffle, Int. Commun. Heat and Mass Transfer, 32 (2005) 94-106.
- Tsay, Y.L., Cheng, J.C., Chang, T.S. 2003. Enhancement of heat transfer from surface-mounted block heat sources in a duct with baffles, Numer. Heat Transfer, Part A, 43, 827-841.
- Zhou, Y. C., Patnaik, B. S. V., Wan, D. C. and Wei1, G. W. 2003. DSC solution for flow in a staggered double lid driven cavity", Int. J. Numer. Meth. Engng. 57, 211-234.